Supplementary Information

Domain wall propagation and pinning induced by current pulses in cylindrical modulated nanowires

C.Bran[1], J.A. Fernandez-Roldan[2], J. A. Moreno[3], A. Fraile Rodríguez[4,5], R. P. del Real[1], A. Asenjo[1], E. Saugar[1], J. Marqués-Marchán[1], H. Mohammed[3], M. Foerster[6], L. Aballe[6], J. Kosel[3,7], M. Vazquez[1], O. Chubykalo-Fesenko[1]

[1] Instituto de Ciencia de Materiales de Madrid, 28049 Madrid, Spain

[2] Helmholtz-Zentrum Dresden-Rossendorf e.V., Institute of Ion Beam Physics and Materials Research, Bautzner Landstrasse 400, 01328 Dresden, Germany

[3] King Abdullah University of Science and Technology, Computer Electrical and Mathematical Science and Engineering, Thuwal 23955-6900, Saudi Arabia.

[5] Departament de Física de la Matèria Condensada, Universitat de Barcelona, Barcelona, 08028, Spain

Institut de Nanociencia i Nanotecnologia (IN2UB), Universitat de Barcelona, Barcelona, 08028, Spain

[6] ALBA Synchrotron Light Facility, CELLS, Barcelona, 08290, Spain

[7] Sensor Systems Division, Silicon Austria Labs, Villach 9524, Austria

Sample preparation. Modulated pores are produced by pulsed hard anodization in oxalic aqueous solution. By tuning the electrochemical parameters periodically geometrical modulations were imprinted along the nanopores length. The templates with modulated pores were obtained in oxalic aqueous solution (0.3M) containing 5 vol.% ethanol at a constant temperature of 0 ºC. During anodization, a constant voltage of 80 V was first applied for 400 s to produce a protective aluminum oxide layer at the surface of the disc which avoids breaking or burning effects during subsequent pulsed hard anodization (Fig.S1a-(I)). In the second step, the voltage was steadily increased (0.08 V/s) up to 130V and kept constant for 400s, which ensures the alignment of the nanochannels (Fig.1(a)-(II)). Nanopores with tailored periodical diameter modulations were produced in step III by applying pulses of 130V and 100V for 5 and 50 s, respectively (Fig. S1-(III)). The pulses were repeated 50 times to obtain a total length of the modulated pores of few tens of microns (Fig.S1 (b)). After an Au nanolayer was sputtered on the back side of the template, Ni magnetic nanowires (Fig. S1 (b)) were grown into the cylindrical modulated pores by electrodeposition taking the shape of already modulated AAO pores [1]. The total length of the nanowires in the membrane is about 28 μm. The cylindrical wires are formed by 500-800 nm long segments with diameter of about 100 nm which are periodically separated by small areas where the diameter is decreased at about 80-90 nm forming geometrical notches along the nanowire´s length (Fig S1 (b)-inset marked in blue). The center-to-center inter-pore distance is kept constant at 320 nm. The variation in the current during anodization (Fig. S1(a)-inset) produces the bottle necks in most of the segments (Fig. S1 (b)-inset and Fig. 1 (b)).

Electrical contacts. The substrates used to contact the single NWs (Fig. S1 (c)-(d)) are 1x1cm^2 Si/SiO_x with 90 ± 5 nm oxide thickness. These were cleaned and then baked at 60 °C

for five minutes in a hotplate in order to remove adsorbed molecules. To prepare a device, a 2μl drop of ethanol containing NWs was released over a substrate right after it was removed from the hotplate and allowed to dry over a permanent magnet. Using a scanning electron microscope (SEM) equipped with a focused ion beam (FIB) this substrate containing NWs was inspected in search for an isolated NW near the center of the substrate. Such NW was signaled by etching marks parallel to its long axis (100 μm away). In order to pattern the contacts over the NW, a two-step lithographic process was used in which LOR5B and AZ5214 photoresists were used sequentially to create an undercut and ease lift-off [2].

To deposit the metallic contacts over the developed samples, a sputtering setup with load-lock plasma etching capabilities was used. Under a base pressure of 10^{-7} Torr, the samples were etched in the load-lock in order to remove the naturally formed oxide layer of the NW and without removing the vacuum, they were transferred to the sputter chamber where 10 nm of chromium and 180 nm of gold were deposited as electrical contacts. Finally, the photoresists (and excess sputtered materials) were lifted-off by submerging in two sequential baths of preheated Remover PG at 60 °C for at least four hours, dipped in IPA, DI water and nitrogen blow dry.

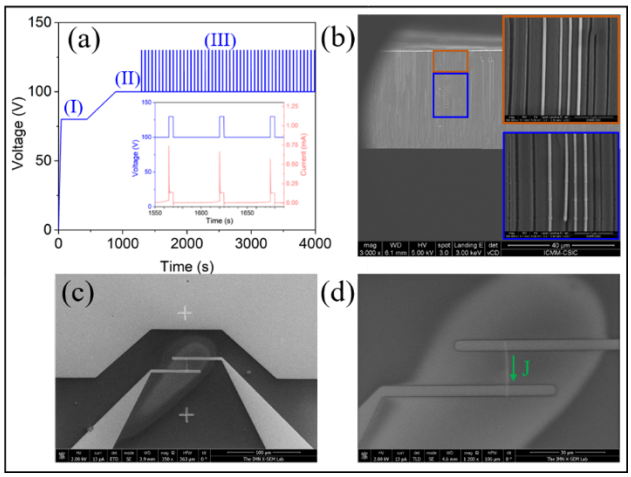

Figure S1. (a) Voltage–time transients of the anodization, including the first anodization step (I), ramping of voltage and keep it constant (II) and the applied pulses (III). The inset shows a close look of both, applied voltage and current transients, during the pulsed anodization (b) SEM image of Ni modulated nanowire embedded in alumina template, (c) Cr/Au electrical contacts, (d) contacted Ni modulated nanowire.

Figure S2 presents the x-ray absorption spectroscopy (XAS) image and XMCD-PEEM images of the Ni modulated nanowire. In (b) the NW is imaged in the as-prepared state showing two domain walls, one of them pinned at the modulation (6), the other one outside the modulation's region. After an intermediate current pulse of $5x10^{11}$ A/m^2 was applied, they move along the current and the nanowire gets saturated as can be observed from the uniform dark contrast in Fig. S2(c).

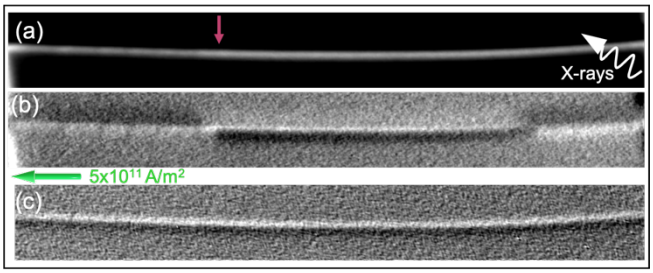

Figure S2. (a) XAS and XMCD-PEEM image of Ni nanowire in as-prepared state (b) and (c) after an intermediate current pulse of 5x10^{11} A/m^2 was applied.

Micromagnetic modelling

a) Simulations of Bloch Point DWs.

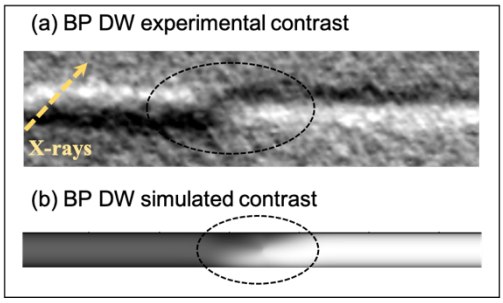

Figure S3. Bloch-point domain wall (BP DW) observed experimentally by XMCD-PEEM (a) and simulated XMCD contrast of a BP DW (b).

Figure S3 presents a comparison between the experimentally observed BP DWs (a) and the simulated XMCD-PEEM contrast of a BP DW (b). The simulations reproduce all features of the experimental contrast, thereby confirming the observation of BP DWs in Ni modulated nanowires.

b) Modelling Joule heating in an individual straight Ni nanowire:

The temperature distribution along the NW axis for different electrical current density values was evaluated with COMSOL Multiphysics® [3] simulations. The geometry of the simulated device was the same as the experimental set-up. The electrical conductivity σ_e as a function of the temperature *T* of the nickel NW was extracted from [4], and the values above room temperature were extrapolated following the equation $\sigma_e = A + B/T + C/T^2 + D/T^3$, where $A = (-1.6 \pm 0.7) \cdot 10^5\ \Omega^{-1} \cdot \mathrm{m}^{-1}$, $B = (1.22 \pm 0.04) \cdot 10^9\ \mathrm{K} \cdot \Omega^{-1} \cdot \mathrm{m}^{-1}$, $C = (-1 \pm 7) \cdot 10^9\ K^2 \cdot \Omega^{-1} \cdot \mathrm{m}^{-1}$, $D = (4.8 \pm 0.4) \cdot 10^{11}\ K^3 \cdot \Omega^{-1} \cdot \mathrm{m}^{-1}$. The thermal conductivity k of the NW was extracted from the electrical conductivity using the Wiedemann-Franz law $k/\sigma_e = L \cdot T$, where L is the Lorenz number and is set to $2.8 \cdot 10^{-8}\ \mathrm{W}\Omega/\mathrm{deg}^2$ [4]. The rest of parameters were extracted from COMSOL library.

Electrical current pulses with amplitudes j_0 from 1 x 10^{11} to 1 x 10^{12} A/m^2 follow the equations $j_{rise} = j_0\left(1 - e^{-t/2}\right)$ and $j_{fall} = j_0\left(e^{-(t-t_p+\tau)/2}\right)$, where j_{rise} and j_{fall} are the rise and fall curves of the pulse, t is the time, t_p = 15 ns is the total pulse duration, and τ = 7 ns the rise time. This shape of the pulse (Figure S4) is chosen in order to assume the deformation of the squared pulse [5].

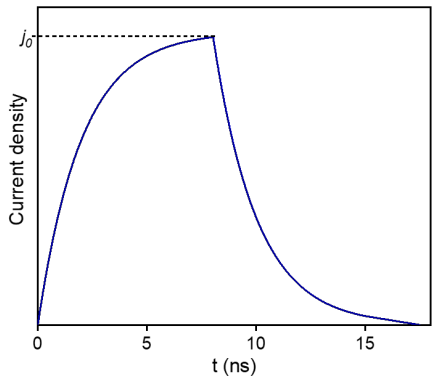

Figure S4. Electrical current pulse used in COMSOL simulations.

c) Current-induced domain wall dynamics and pinning in modulated nanowires.

In order to understand the magnetization processes observed in the XMCD-PEEM experiment, we have investigated the dynamics of a domain wall in a Ni nanowire with a total length 2L = 5 μm, a diameter of D_o=100 nm, and periodical notches given by a nanowire width

$$D(z) = D_o - \Delta\left(\operatorname{sech}\left(\frac{x}{w}\right) + \operatorname{sech}\left(\frac{x+L}{w}\right) + \operatorname{sech}\left(\frac{x-L}{w}\right)\right) \quad (1)$$

as a function of the axial coordinate $x \in (-L, L)$. $\Delta = 12$ nm and w=16 nm are adequate values to approach the dimensions observed in the SEM images. In this approach the notches, labelled from 1 to 3, are spaced by 500 nm as depicted in Fig S5(a). The magnetization is colored by its axial component.

We integrated LLG equation to solve the magnetization dynamics of a pre-nucleated Bloch Point domain wall. Current interacts with the reduced magnetization $\boldsymbol{m}$ through the Zhang-Li spin transfer torque $\boldsymbol{\tau}_{ZL}$ and the Oersted field produced by the current following the model[39]

$$\boldsymbol{\tau}_{\mathrm{ZL}} = \frac{1}{1+\alpha^2}\Big((1+\xi\alpha)\ \boldsymbol{m}\times(\boldsymbol{m}\times(\boldsymbol{v}\cdot\nabla)\boldsymbol{m}) + (\xi-\alpha)\boldsymbol{m}\times\big((\boldsymbol{v}\cdot\nabla)\boldsymbol{m}\big)\Big) \quad (2)$$

where $\boldsymbol{v} = \frac{P\,\mu_B}{2\,e\,\gamma_0 M_S\,(1+\xi^2)}\boldsymbol{J}$, $\boldsymbol{J}$ is the current density, α is the magnetization damping, ξ is the degree of non-adiabaticity, μ_B is the Bohr magneton, e is the elementary charge, γ_0 is the gyromagnetic ratio, M_S is the saturation magnetization, and *P* is the current polarization. The Oersted field has been precalculated using analytical expressions from the model introduced in section (d) in SI.

The implementation is carried out with the finite different package mumax3 [6] (version 3.10) and cell size 1x1 nm. We used typical parameters of Ni in Table 1. Magnetic poles have been removed from the ends of the nanowire to mimic long wire conditions in the demagnetizing field. We introduced the pre-calculated Oersted field (3),(4) for a current flow through a nanowire with profile $D(z)$ in Eq. 1. The spin-polarized current has a polarization P=0.5, non-adiabaticity ξ=0.1 and damping 0.02. Exchange, complete magnetostatic and cubic anisotropy (with one of the easy axis parallel to the nanowire axis) contributions are included. The Landau-Lifshitz-Gilbert equation of motion with additional term (2) is solved.

Table 1. Material parameters and crystal structural in micromagnetic modelling.

Material	$\mu_o M_s$ (T)	A_{ex} (pJ/m)	Crystal Symmetry	K_1 (kJm^{-3})	Magnetization Easy Axis (e.a.)

Ni [7]	0.61	3.4	Cubic	-4.8	crystal lattice direction parallel to the nanowire axis

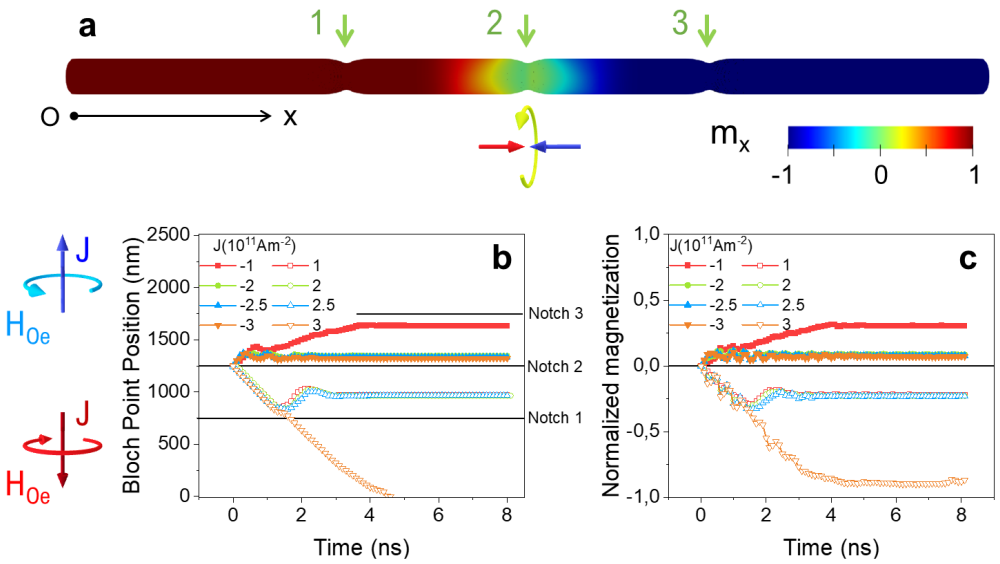

Figure S5. Initial Bloch Point Wall configuration in a Ni nanowire with three notches (a). The green arrows indicate the position of the notches from 1 to 3, the schematic view below the wire represents the Bloch Point wall structure. (b)The position of the Bloch point as a function of time during propagation under current in the nanowire for various current density values (c) Normalized axial magnetization component as a function of time for the same current density values. A vast panorama of dynamic and pinning processes which cannot be accurately interpreted from the 'wavy' magnetization dynamics, reflecting spin-wave emission.

We start with a pre-nucleated head-to-head Bloch Point Domain Wall (BP DW) at the notch 2 as indicated in Figure S5(a). To track the BPDW dynamics, we follow both the axial component of the magnetization $m_x(t)$ as well as the BP position, which is determined by the intersection of three iso-surfaces (m_x=0, m_y=0, m_z=0). In this example the direction of the Oersted field for positive currents has the same sense as the azimuthal component of the magnetization of the domain wall, i.e., the BP DW has a 'good chirality'.

The dynamics start immediately with the switching ON of a current pulse of density J and its Oersted field. It is important to bear in mind that the temporal dependence of the position of the BP DW and the mean magnetization in the wire in Figures S5(b-c) are strictly not proportional one to another mainly due to the emission of spin waves during the dynamics which is observed in Fig S5(c). In regard to the position of the BP DW for positive currents in Figure S5(b), we observe that the propagation of the Bloch Point occurs in the direction opposite to the direction of current (indicated by blue arrow of J on the left side of the graph). This result is general for negative and positive currents in Figures S5(b-c).

The BP DW can pass the notch only for high current densities (>$3\cdot10^{12}$ A/m^2). For lower current density the BP DW remains pinned at some position. Strikingly, the pinning position is the same for every pinned Bloch Point irrespectively of the value of the current density.

d) General expressions for current density and Oersted field in modulated cylindrical nanowires.

The Oersted field $\mathbf{H_{Oersted}}$ induced by the current has been analytically pre-calculated in an infinitely long straight cylindrical wire with modulations in diameter to generalize the model in Ref 39 in the main text.
Consider the nanowire profile $r = R(z)$ in Fig. S6(a) and cylindrical coordinates (r,ϕ,z) with a coordinate cylindrical basis $\{\overrightarrow{u_r}, \overrightarrow{u_\phi}, \overrightarrow{u_z}\}$ and a z-axis colinear with the axis of the wire. Due to the revolution symmetry, the azimuthal component of the current density is zero, I,e.

$$\vec{J} = J_r(r,z)\overrightarrow{u_r} + J_z(r,z)\overrightarrow{u_z} \qquad (1).$$

Furthermore,

- In the stationary regime there is no charge accumulation in the ends of the wire, and current lines cannot cross so the continuity equation becomes
$$\vec{\nabla} \cdot \vec{J} = 0 \qquad (2)\ .$$
- Boundary conditions on the surface imply $\vec{n} \cdot \vec{J}|_{surface} = 0$ at $r = R(z)$, and thus
$\frac{J_r}{J_z}|_{r=R(z)} = \frac{dR}{dz}$ (3)
at the surface $r = R(z)$.

- The total current flowing through the cross section $S(z)$ in the wire is
$$I = \int_{cross\ section} \vec{J} \cdot dS = J_z S(z) \qquad (4).$$

Solving Eq. (2) with Eqs. (3) and (4) and the conditions $J_r(r = 0, z) = 0$ at every z position leads to a general expression for the current density for the nanowire profile

$$J_z(z) = \frac{I}{S(z)} = \frac{I}{\pi R^2(z)} \qquad (5)$$

$$J_r(r,z) = \frac{r}{2}\frac{I}{S(z)^2}\frac{dS(z)}{dz} = r\frac{I}{\pi R^3(z)}\frac{dR}{dz} \qquad (6)$$

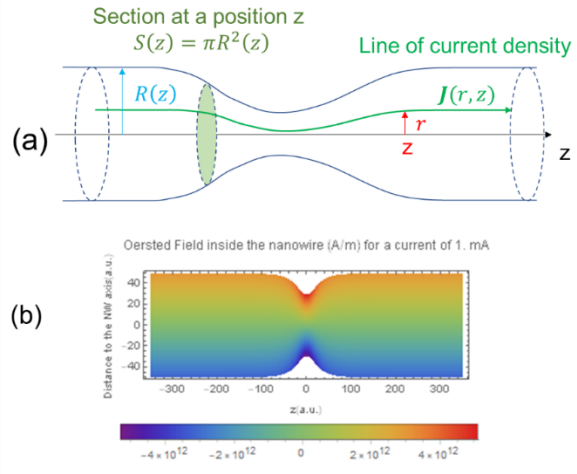

Figure S6. Profile of an axially-symetric nanowire with modulated profile. A stationary current density flows from the left end to the right end.

The integration of the Oersted field for our nanowire simplifies considering from Biot-Savart expression $\vec{H} = \frac{1}{4\pi}\int dv\, \vec{J} \times \frac{\vec{r} - \overrightarrow{r'}}{|\vec{r} - \overrightarrow{r'}|^3}$ and that the vector product $\vec{J} \times \vec{r} - \overrightarrow{r'}$ leads only to

contributions in $\overrightarrow{u_\phi}$ owing to the revolution symmetry, either inside (r<R(z)) or outside (r>R(z)) the wire. Thus $\overrightarrow{H_{Oe}} = H_\phi(r,z)\overrightarrow{u_\phi}$.

Maxwell equations in the estationary case simplifies to

$$\vec{\nabla} \times \vec{H} = 0 \qquad (7),$$

that can be solved for a long wire together with Eq. (5) and (6) with the condition of a long wire (Jr has no contribution inside the wire (r>R(z)). To solve (7) ouside the wire (r>R(z)) we use the continuity conditions for the magnetic field at the surface $\vec{n} \times \left(\overrightarrow{H_{r<R(z)}} - \overrightarrow{H_{r>R(z)}}\right)|_{r=R(z)} = 0$.

As a result, the Oersted field induced by a estationary current for an arbitrary nanowire profile is

$$\overrightarrow{H_{Oe}} = \frac{I}{S(z)}\frac{r}{2}\overrightarrow{u_\phi} = \frac{I}{\pi R^2(z)}\frac{r}{2}\overrightarrow{u_\phi} \text{ for } r \le R(z) \qquad (8).$$

$$\overrightarrow{H_{Oe}} = \frac{R^2(z)}{2r}J_z(z)\overrightarrow{u_\phi} = \frac{I}{2\pi r}\overrightarrow{u_\phi} \text{ for } r > R(z) \qquad (9).$$

Expressions (8) and (9) are introduced in mumax3 to compute the Oersted field at each point in ideal conditions. These expressions allow recovering the model of Ref. 39 in the main text in the case of R(z)=cte.

e) *Simulations of the nucleation during the application of current pulses of high densities*

This simulations have been performed with the aim to assess the miinimum current density required for thermal domain wall nucleation during the actuation of the current pulse.

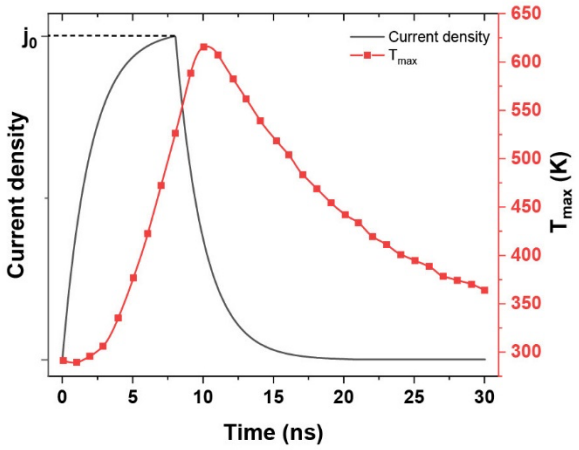

Figure S7. Typical temperature dynamics evaluated by COMSOL for current density j=8 10^{11} A/m^2

Simulations have been performed using the stochastic Landau-Lifshitz-Bloch (LLB) methodology [8,9] which does not conserve the magnetization magnitude and allows variable temperature profile with temperatures close and above the Curie temperature (Fig.S7). The magnetization as a function of temperature is taken from the Langevin function. For simplicity, we assumed a squared temperature profile for given current density with the same maximum temperature as the one obtained by the COMSOL Multiphysics software which lasts 50 ns. This assumption will re-enforce nucleation. The micromagnetic parameters used in the simulations are T_c = 628 K, $M_s(T = 0)$ = 0.61 T, $A(T = 0) = 9 \cdot 10^{-12}$ Jm^{-1} and $K_u(T = 0)$ = 4.8 kJm^{-3}. We assumed the Callen-Callen law for temperature dependence of the anisotropy

proportional to m^{10} and a temperature dependence of the exchange parameter proportional to $m^{1.76}$[10], where m is the reduced magnetization. The simulations start with a saturated nanowire at T=300K, after which the free energy is minimized by solving the LLB equation. For simplicity, distribution of temperature along nanowire was considered to be uniform. The discretization size was chosen to be 2 nm.

References:

[1] C. Bran, J. A. Fernandez-Roldan, R. P. del Real, A. Asenjo, O. Chubykalo-Fesenko, and M. Vazquez, Magnetic Configurations in Modulated Cylindrical Nanowires, Nanomaterials 11, 600 (2021). DOI: 10.3390/nano11030600.

[2] H. Mohammed, J.A. Moreno, and J. Kosel, Advanced fabrication and characterization of magnetic nanowires. *Magnetism and Magnetic Materials*, *2*, pp.137-164 (2017).

[3] COMSOL Multiphysics® v. 6.0. www.comsol.com. COMSOL AB, Stockholm, Sweden.

[4] M.N. Ou et al. Electrical and thermal transport in single nickel nanowire. Appl. Phys. Lett. 92, 063101 (2008)

[5] M. Schöbitz et al., Supplementary material for Fast domain wall motion governed by topology and Oersted fields in cylindrical magnetic nanowires, Phys. Rev. Lett. 123, 217201 (2019)

[6] Vansteenkiste, A.; Leliaert, J.; Dvornik, M.; Helsen, M.; Garcia-Sanchez, F.; Van Waeyenberge, B. The Design and Verification of MuMax3. AIP Adv. 2014, 4 (10), 107133.https://doi.org/10.1063/1.4899186.

[7] Y. Liu, D.J. Sellmyer, D. Shindo, Eds., Handbook of Advanced Magnetic Materials, Vol. 1: Springer, Berlin, 2006.

[8] N. Kazantseva, D. Hinzke, U. Nowak, R. W. Chantrell, U. Atxitia, O. Chubykalo-Fesenko, Phys. Rev. B 2008, 77 (18), 184428.

[9] R. F. L Evans,D. Hinzke, U. Atxitia, U. Nowak, R. W. Chantrell, O. Chubykalo-Fesenko, Phys. Rev. B 2012, 85 (1), 014433.

[10] U. Atxitia, D. Hinzke, O. Chubykalo-Fesenko, U. Nowak, H. Kachkachi, O. N. Mryasov, R. F. Evans, and R. W. Chantrell Phys. Rev. B 82, 134440 (2010)